

Remote-Powered High-Performance Strain Sensing Microsystem

Michael Suster, Nattapon Chaimanonart, Jun Guo, Wen H. Ko, and Darrin J. Young
EECS Department, Case Western Reserve University, Cleveland, Ohio

Abstract

This paper presents an RF remote-powered high-performance strain sensing microsystem. A MEMS capacitive strain sensor converts an input strain to a capacitance change, followed by low-noise integrated sensing electronics converting the capacitive signal to an output voltage with an overall sensitivity of $420 \mu\text{V}/\mu\epsilon$. An RF to DC converter based on inductive coupled coils converts a 50 MHz AC signal to a stable DC supply of 2.8 V with a current driving capability of 2 mA, sufficient to power the interface sensing electronics. The prototype microsystem achieves a minimum detectable strain of $0.09 \mu\epsilon$ over a 10 kHz bandwidth with a dynamic range of 81 dB. The sensing electronics consume 1.5 mA from a 2.8 V supply.

Introduction

High-performance wireless strain sensing microsystems are critical for advanced industrial applications, such as point-stress and torque sensing for ball-bearings and rotating shafts and blades. Stringent performance requirements with a high sensitivity of 0.1 micro-strain ($\mu\epsilon$) over a wide bandwidth of 10 kHz and a large dynamic range of 80 dB are demanded for these applications. Conventional strain sensors made of metal foils and semiconductor piezoresistive elements suffer from a limited sensitivity, large temperature dependence, turn-on drift, and poor time stability, thus inadequate for high-performance applications [1, 2]. MEMS resonant strain sensors [3] have been demonstrated to achieve a high performance by converting an input strain to a change in the device resonant frequency, but requires a large operating voltage of a few tens of volts, thus undesirable for low voltage and low power integrated systems. MEMS capacitive strain sensors, however, are attractive due to a number of key advantages such as high sensitivity, minimum temperature dependence and turn-on drift, low noise, large dynamic range, and potential monolithic integration with CMOS electronics [4, 5], and thus will be employed for the prototype microsystem design.

Industrial strain sensing applications further impose significant design challenges due to various rotating mechanical components employed in the system. Therefore, stand-alone wireless sensing microsystems with remote powering and data telemetry capabilities are highly desirable. Inductive-coupling-based powering techniques have been widely used for biomedical implants [6, 7]. In these applications, the coupling coils are placed at certain fixed positions with a short distance on the order of a few millimeters. It is, therefore, necessary to develop remote powering systems, which are insensitive to mechanical rotations and can achieve an increased coupling distance for advanced industrial sensing applications.

In this paper, an RF remote-powered MEMS capacitive strain sensor and low-noise sensing electronics for high-

performance applications is presented. A MEMS capacitive strain sensor and CMOS sensing electronics achieve a dynamic range of 81 dB with a strain resolution of $0.09 \mu\epsilon$ over a 10 kHz bandwidth. An RF remote powering system, consisting of rotation-insensitive coupling coil loops and integrated CMOS power conversion electronics, achieves a stable DC output voltage of 2.8 V with a 2 mA current supply capability to power the sensing electronics.

Microsystem Architecture

Figure 1 presents a proposed stand-alone microsystem architecture, which consists of a MEMS capacitive strain sensor and interface electronics with coil loops for remote powering and data telemetry. The microsystem is attached to the surface of a rotating iron shaft with a diameter of 3 inches for the prototype design. An internal coil is wound around the shaft and separated from the external coil by one inch. This configuration is critical for achieving a stable and uniform coil coupling during shaft rotation. The rotation of the shaft produces a rotational torque, thus a surface strain, which can be sensed by the MEMS strain sensor. The sensor output is then converted to an analog voltage, followed by digitization and data telemetry to a nearby receiver for signal acquisition and analysis. This paper focuses on the design and performance characterization of a MEMS strain sensor, low noise interface electronics, and a remote RF powering system. The sensor data telemetry system is currently under development.

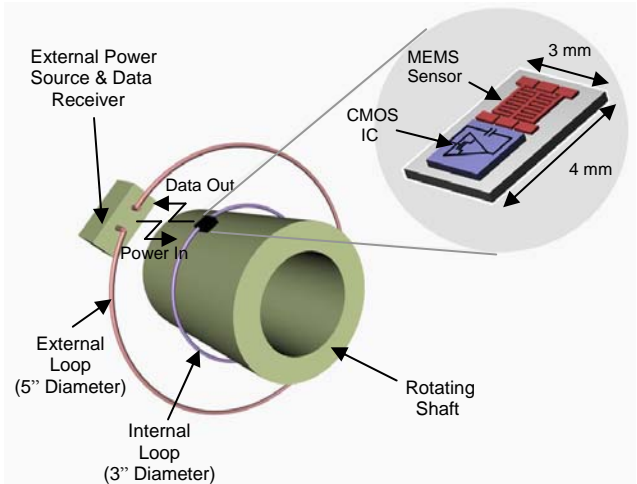


Figure 1. Stand-alone wireless strain sensing microsystem architecture

MEMS Strain Sensor

Figure 2 shows a simplified schematic of a MEMS capacitive strain sensor employed in the prototype system. The device consists of three amplifying buckled beams, critical for improving device sensitivity, with comb fingers positioned at the structural center. An externally applied strain introduces a small lateral displacement, Δx , which will result in an enhanced beams deflection along the vertical

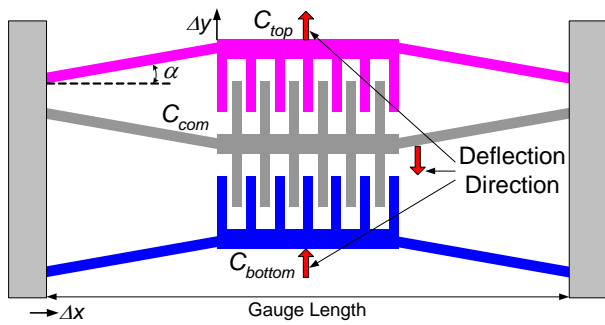


Figure 2. MEMS capacitive strain sensor

axis, upward for the C_{top} and C_{bottom} beams and downward for the center beam, C_{com} . The C_{top} and C_{bottom} electrodes thus form a set of linear differential capacitors (C_s^+ and C_s^-) with respect to the C_{com} electrode, serving as a common reference electrode as shown in the figure. Optimized sensors exhibit a buckling angle of 5.7° , a structural thickness of $20\ \mu\text{m}$, a minimum air gap size of $3.6\ \mu\text{m}$, and a lateral gauge length of $1\ \text{mm}$ with 37 sets of center-positioned fingers. The sensors have been fabricated by using DRIE on SOI substrates followed by releasing to free the microstructures [4]. Four fabricated sensors connected in parallel as shown in Figure 3 achieve a nominal capacitance value of $0.44\ \text{pF}$ with a differential sensitivity of $265\ \text{aF}/\mu\epsilon$. Mechanical thermal noise, commonly referred to as Brownian motion, for the sensor is estimated several orders of magnitude lower than the minimum detectable signal requirement when operated in air. Therefore, the sensor does not require a costly vacuum packaging, and low-noise sensing electronics are critical for achieving the overall stringent system performance requirements.

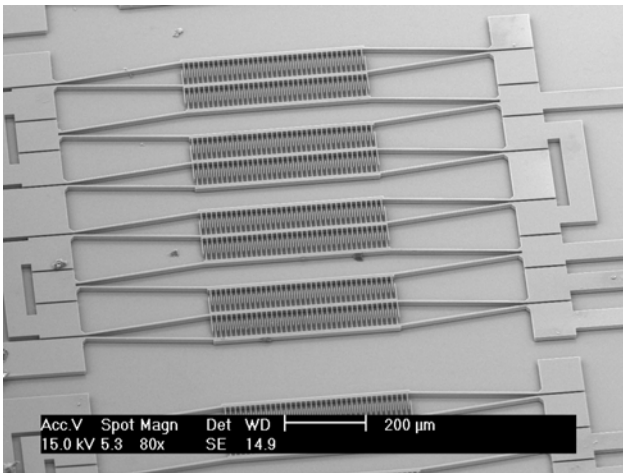


Figure 3. SEM of fabricated strain sensors

Low-Noise Interface Electronics

Figure 4 shows the architecture of the low-noise continuous-time synchronous detection interface electronics employed in the prototype system [8]. The MEMS sensors, modeled as differential capacitors, are driven by a clock signal with an amplitude of $1.2\ \text{V}$ and interfaced by a differential charge amplifier, which converts the sensor capacitance change to an output voltage. A clock frequency of $1\ \text{MHz}$ is chosen to modulate the sensor information away

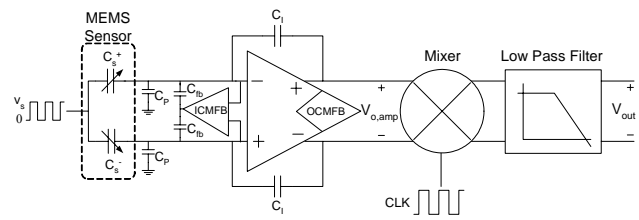


Figure 4. Electronic strain sensing architecture

from the $1/f$ noise of the amplifier, a critical means to achieve a high sensitivity. An input common-mode feedback (ICMFB) circuit is incorporated with the charge amplifier to minimize its input common-mode shift caused by the driving clock; hence, suppressing any offset signal due to the parasitic capacitance mismatch and drift over time. Feedback capacitors, C_{fb} , of $1.4\ \text{pF}$ each are chosen to sufficiently compensate the common mode shift. The charge amplifier output is then mixed by the same clock signal and low-pass filtered to obtain the desired strain information.

The integrating capacitor, C_i , of $1.6\ \text{pF}$ is chosen to achieve an output signal range from $20\ \mu\text{V}$ to $200\ \text{mV}$, corresponding to the minimum and maximum input strain of $0.1\ \mu\epsilon$ and $1000\ \mu\epsilon$ ($80\ \text{dB}$ dynamic range), respectively. This voltage range is determined by the mixer input signal range. The overall parasitic capacitance, C_p , consisting of capacitances from the sensor interconnect, wire bonding pads, and amplifier input capacitance is estimated to be $3\ \text{pF}$. Therefore, an input referred noise spectral density of $5\ \text{nV}/\sqrt{\text{Hz}}$ is required for the charge amplifier to achieve an SNR of approximately 3 at the mixer output with the minimum input strain signal. A fully differential charge amplifier is designed with an input transconductance of $1\ \text{mS}$ to achieve the required noise specification [8].

A fully differential switching mixer is designed to achieve a conversion gain of 3.3 with a negligible noise contribution. A second-order low-pass filter with a cut-off frequency of $80\ \text{KHz}$ is implemented to obtain a linear phase characteristic to ensure an un-distorted time-domain signal waveform over the required bandwidth. The overall interface electronics consume $1.5\ \text{mA}$ of DC current from a $2.8\ \text{V}$ supply.

Remote RF Powering System

Figure 5 presents the proposed remote RF powering architecture [9], where an external RF power source is used to drive a tuned series resonator consisting of L_1 and C_1 . The resonator is tuned to an optimal frequency as will be illustrated. The RF signal is coupled to a parallel resonator, consisting of L_2 and C_2 , tuned to the same frequency. The

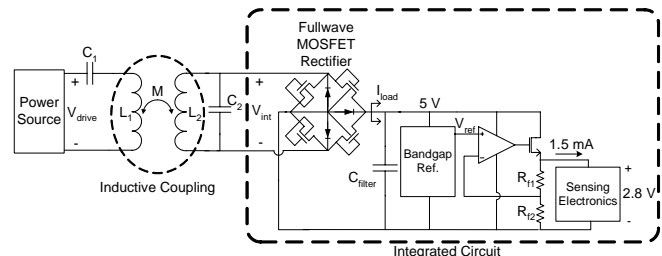


Figure 5. Remote RF powering system architecture

signal is then rectified by an integrated CMOS fullwave rectifier to 5 V and further regulated to achieve a stable 3 V DC supply with a 2 mA current driving capability, sufficient to power the interface electronics. In order to achieve an efficient power conversion system, the voltage gain across the tuned resonator network needs to be maximized. The gain can be expressed as

$$\frac{V_{int}}{V_{drive}} = \frac{\omega^2 L_2 M}{(R_1 R_2 + (\omega M)^2 + R_1 (\omega L_2)^2 / R_{load})}, \quad (1)$$

where M represents the mutual inductance between L_1 and L_2 , ω is the angular operating frequency, R_{load} is the equivalent AC resistive loading of the rectifier, which is equal to 1.4 k Ω due to the system design requirements, and R_1 and R_2 are series resistances associated with the series and parallel resonators, respectively. In the prototype design R_1 is 12 Ω , which is dominated by the output resistance of the power source. For a fixed internal coil diameter of 3 inches, L_1 , L_2 , M , and R_2 are a function of the number of coil turns and operating frequency. These parameters have been extensively characterized to obtain an optimal condition for achieving a maximum voltage gain. Figure 6 presents the measured voltage gain as a function of frequency and internal coil turn number, which closely matches the predicted performance from Equation (1). It can be seen that

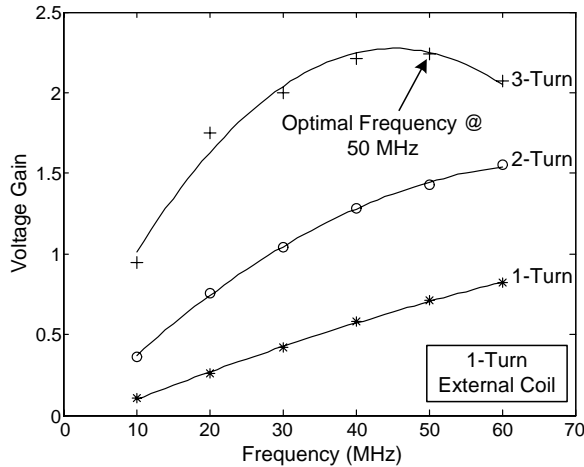


Figure 6. Measured voltage gain frequency response for different internal coil turn numbers

a maximum voltage gain of 2.25 can be achieved at a 50 MHz operating frequency with a one-turn external coil loop, exhibiting an inductance value of 320 nH and AC resistance of 0.8 Ω , and a three-turn internal coil loop with an inductance value of 450 nH and AC resistance of 9.4 Ω . Both coil loops have self resonant frequencies well above 100 MHz and exhibit a mutual inductance of 25 nH. A design employing a four-turn internal coil loop suffers from a reduced voltage gain due to an excessive iron core loss at high frequencies. Experiments have also shown that a design with a two-turn external coil can achieve a comparable gain. However, a much reduced operating frequency is required, limited by the self resonant frequency of the external coil. The reduced frequency will call for an excessively large on-chip filter capacitor for ripple suppression, thus unattractive for microsystem implementation.

An integrated CMOS fullwave rectifier is used to rectify the received RF signal, as shown in Figure 5. The rectifier is implemented by four MOSFETs connected in a diode configuration along with their parasitic source and drain to bulk junction diodes. The input to the rectifier, V_{int} , is the coupled RF signal across the parallel resonator, which is to be rectified to produce a 5 V DC output. The total voltage drop across the rectifier is approximately 2.7 V. Therefore, an RF signal with a 7.7 V amplitude is required to obtain a DC output voltage of 5 V. A filtering capacitor, C_{filter} , provides ripple suppression. The ripple on the 5 V line is inversely proportional to the filter capacitance value and operating frequency. The prototype microsystem employs a 400 pF filtering capacitor, occupying a chip area of 0.9 mm x 0.9 mm, for a peak-peak ripple voltage of 60 mV at the 5 V line, determined by the system design requirements.

A CMOS linear regulator is used in the prototype system to regulate the 5 V line to a stable DC voltage of 3 V. The linear regulator compares the output voltage through a resistive feedback network, consisting of R_{f1} and R_{f2} , to a stable bandgap reference voltage, V_{ref} , of 1.25 V with a high-gain inverting amplifier, as shown in Figure 5.

Measurement Results

Figure 7 shows the chip photo of the fabricated CMOS RF-DC power converter and MEMS sensor interface electronics using a 1.5 μm CMOS process. The MEMS sensor chip is wire bonded to the sensing electronics to form the prototype system as shown in Figure 8. The sensor chip is then subjected to a three-point strain testing process for system characterization. Figure 9 shows the measured output

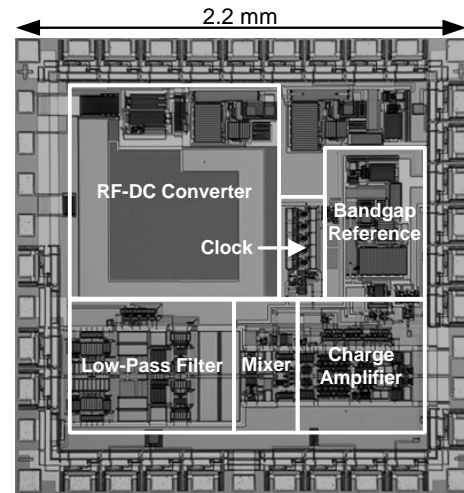


Figure 7. Fabricated chip photo

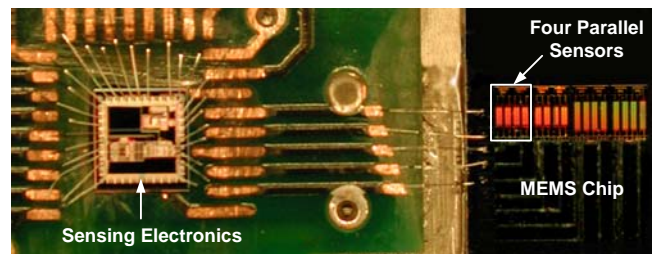


Figure 8. Prototype system testing board

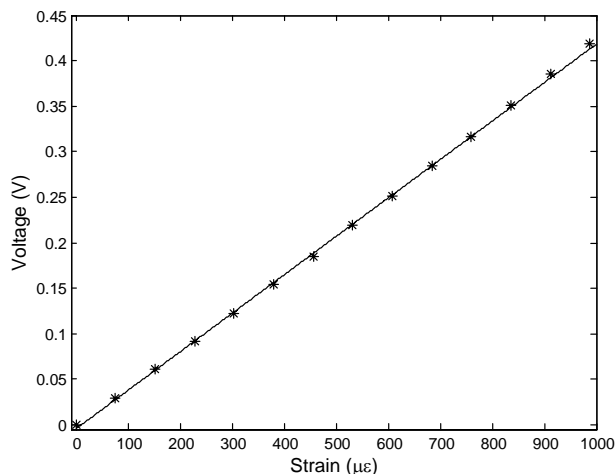


Figure 9. Output voltage vs. input strain

voltage versus an applied input strain, indicating that the prototype system can achieve a maximum input signal of 1000 $\mu\epsilon$, corresponding to an output voltage of 420 mV, with a linearity of 1.5% of full scale.

The remote RF powering system is tested by driving the tuned LC network with a 50 MHz RF power source with an amplitude of 8 V peak-to-peak, as shown in Figure 10. For testing purposes, the CMOS chip is packaged in a DIP40 through-hole package and mounted on the surface of an iron shaft. The system provides a stable DC voltage of 2.8 V (due to the modeling limitation of the junction diodes used in the bandgap reference design) with a 2 mA current supply capability independent of the iron shaft rotation.

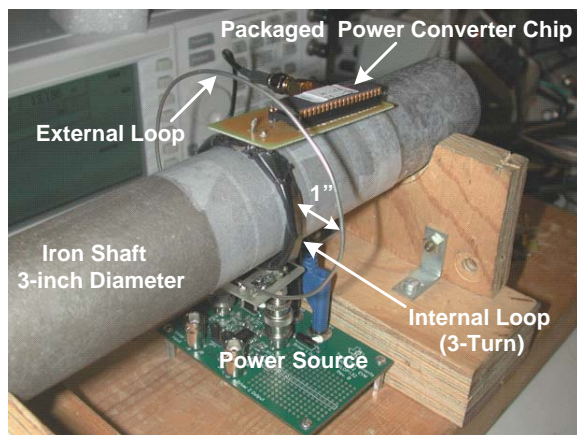


Figure 10. Remote RF powering system test setup

Figure 11 presents the measured output noise spectral density when the interface electronics are powered by the remote-powering system, demonstrating that the microsystem achieves a low noise level of $380 \text{ nV}/\sqrt{\text{Hz}}$, which is equivalent to a minimum detectable signal of 38 μV , or 0.09 $\mu\epsilon$, over a 10 KHz bandwidth, thus an 81 dB dynamic range. The low frequency tone around 500 Hz and $1/f$ noise are contributed by the measurement equipment.

Conclusion

An RF remote-powered high-performance strain sensing microsystem has been demonstrated. A MEMS capacitive strain sensor and low-noise continuous time synchronous

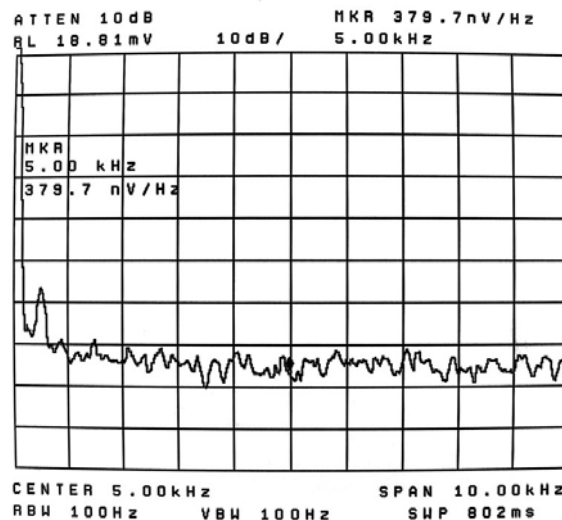


Figure 11. Output noise spectral density

detection electronics achieve stringent system performance requirements. The interface electronics are powered by a remote RF powering system, which is independent of mechanical rotation. The prototype system demonstrates a strain sensing resolution of 0.09 $\mu\epsilon$ over a 10 kHz bandwidth with 81 dB dynamic range. The demonstrated performance represents two orders of magnitude improvement compared to any existing commercial strain sensing technologies.

Acknowledgements

This work is partially supported by the U.S. Army Research Office under contract # DAAD19-02-1-0198.

References

- [1] M. L. Nagy, C. Apanius, and J. W. Siekkinen, "A user friendly, high-sensitivity strain gauge," *Sensors*, Vol. 18, pp. 20–27, June 2001.
- [2] M. Hrovat, D. Belavic, Z. Samardzija, and J. Holc, "An investigation of thick-film resistor, fired at different temperatures, for strain sensors," *International Spring Seminar on Electronics Technology*, May 2001, pp. 32-36.
- [3] K. E. Wojciechowski, B. E. Boser, and A. P. Pisano, "A MEMS resonant strain sensor operated in air," *The Seventeenth Annual International Conference on Micro Electro Mechanical Systems (IEEE-MEMS)*, January 2004, pp. 841-845.
- [4] J. Guo, H. I. Kuo, D. J. Young, and W. H. Ko, "Buckled beam linear output capacitive strain sensor," *Solid-State Sensor, Actuator and Microsystems Workshop*, June 2004, pp. 344-347.
- [5] L. Que, M.-H. Li, L. L. Chu, and Y. B. Gianchandani, "Measurements of material properties using differential capacitive strain sensors," *Journal of Microelectromechanical Systems*, Vol. 11, pp. 489-498, October 2002.
- [6] J. A. Von Arx and K. Najafi, "A wireless single-chip telemetry-powered neural stimulation system," *Technical Digest, IEEE International Solid-State Circuits Conference*, pp. 214–215, February 1999.
- [7] W. Liu and M. S. Humayun, "Retinal prosthesis," *Technical Digest, IEEE International Solid-State Circuits Conference*, pp. 218–225, February 2004.
- [8] M. Suster, J. Guo, N. Chaimanonart, W. H. Ko, and D. J. Young, "Low-noise CMOS integrated sensing electronics for capacitive MEMS strain sensors," *IEEE Custom Integrated Circuits Conference*, October 2004, pp. 693-696.
- [9] N. Chaimanonart, W. H. Ko, and D. J. Young, "Remote RF powering system for MEMS strain sensors," *IEEE Sensors Conference*, October 2004.